Shear-Driven Hydrogen-Air Mixing in OP16 DLE Combustor
A Comparative Study Between URANS and LES

Donepudi, Teja; Pecnik, Rene; Peeters, Jurriaan W. R.; Klein, Sikke; Bouten, Thijs; Axelsson, Lars-Uno

DOI
10.1115/gt2024-123831

Publication date
2024

Document Version
Final published version

Published in
Ceramics and Ceramic Composites; Coal, Biomass, Hydrogen, and Alternative Fuels

Citation (APA)
Donepudi, T., Pecnik, R., Peeters, J. W. R., Klein, S., Bouten, T., & Axelsson, L.-U. (2024). Shear-Driven Hydrogen-Air Mixing in OP16 DLE Combustor: A Comparative Study Between URANS and LES. In *Ceramics and Ceramic Composites; Coal, Biomass, Hydrogen, and Alternative Fuels: ASME Turbo Expo 2024: Turbomachinery Technical Conference and Exposition* Article V002T03A011 (Proceedings of the ASME Turbo Expo; Vol. 2). The American Society of Mechanical Engineers (ASME). https://doi.org/10.1115/gt2024-123831

Important note
To cite this publication, please use the final published version (if applicable).
Please check the document version above.

Proceedings of ASME Turbo Expo 2024
Turbomachinery Technical Conference and Exposition
GT2024
June 24-28, 2024, London, United Kingdom

GT2024-123831

SHEAR-DRIVEN HYDROGEN-AIR MIXING IN OP16 DLE COMBUSTOR: A COMPARATIVE STUDY BETWEEN URANS AND LES

Teja Donepudi[1], Rene Pecnik[1], Jurriaan W. R. Peeters[1], Sikke Klein[1,*], Thijs Bouten[2], Lars-Uno Axelsson[2],

[1]Delft University of Technology, Delft, The Netherlands
[2]Destinus Energy, Hengelo, The Netherlands

ABSTRACT

This paper presents numerical predictions of the flow field in the swirl-stabilized OP16 DLE combustor using hydrogen as a fuel. Computational Fluid Dynamics (CFD) simulations employing unsteady Reynolds-Averaged Navier-Stokes (URANS) and Wall Modelled Large Eddy Simulations (WMLES) are performed without including reaction mechanisms. The objective is to gain insights into scalar mixing predictions of the two approaches when hydrogen and air undergo shear-driven turbulent mixing. Accurate scalar mixing predictions are crucial in the combustors' design process to assess the uniformity of fuel-air mixing as localized regions of high fuel concentrations can lead to increased NOx emissions and to identify locations with a propensity for Boundary Layer Flashback (BLF). Results are compared and analyzed in terms of time-averaged equivalence ratio, unmixedness and Turbulent Kinetic Energy (TKE) profiles. TKE predictions are lower in URANS, leading to significantly lower fuel-air mixing levels than WMLES, indicating differences in their predictions of shear-layer interactions in the mixing region and the swirl section of the combustor.

Keywords: Gas turbine combustion, Hydrogen, Shear Flows, CFD.

NOMENCLATURE

Latin characters

C	Swirler blade chord length [m]
$\mathscr{D}$	Mass diffusion coefficient [$m^2\ s^{-1}$]
H	Total enthalpy [$kgm^2\ s^{-2}$]
k	Turbulent kinetic energy [$kgm^2\ s^{-2}$]
R	Combustor radius [m]
S	Strain rate tensor [s^{-1}]
t	Time [s^{-1}]
u	Velocity [$m\ s^{-1}$]
x, y	Distance [m]
Y	Species mass fraction [-]

Greek letters

ρ	Density [kgm^{-3}]
τ	Viscous force tensor [$kgm^{-2}\ s^{-2}$]
$\mathscr{J}$	Molecular diffusive flux [$kgm^{-2}\ s^{-1}$]
ϕ	Equivalence ratio [-]
δ	Length filter [m]
ω	Turbulent kinetic energy dissipation rate [$m^2\ s^{-3}$]
μ	Dynamic viscosity [$kgm^{-1}\ s^{-1}$]
ψ	Unmixedness [-]

Dimensionless groups

Re	Reynolds number, $\rho u R/\mu$
Sc	Schmidt number, $\mu/\rho\mathscr{D}$

Superscripts and subscripts

i, j	Mutually perpendicular coordinate axis
k	Species
t	Turbulent
f	Fuel
*, +	Non-dimensional values
$\sim$	Favre averaged
"	Favre unknown

Abbreviations

BLF	Boundary Layer Flashback
CFD	Computational Fluid Dynamics
CFL	Courant Friedrichs Lewy
CPU	Central Processing Unit
DLE	Dry Low Emissions
DNS	Direct Numerical Simulations
GPU	Graphics Processing Unit
LES	Large Eddy Simulations
SIMPLE	Semi-Implicit Method for Pressure Linked Equations
SGS	Sub Grid Scale
SRS	Scale Resolving Simulations
SST	Shear Stress Transport
TKE	Turbulent Kinetic Energy
URANS	Unsteady Reynolds Averaged Navier-Stokes
WMLES	Wall Modelled Large Eddy Simulations

*Corresponding author: S.A.Klein@tudelft.nl

1. INTRODUCTION

Global economic growth relies heavily on energy production, primarily sourced from fossil fuels (nearly 80% [1]). Energy production by combustion of these fossil fuels accounts for 44% of the global CO_2 emissions [2] hampering worldwide efforts to achieve near-zero carbon footprint by 2050 [3]. More interestingly, the global economic output and CO_2 emissions simultaneously increased by nearly 6% in 2021, suggesting a strong correlation between them [4]. On the other hand, recent years have witnessed a surge in power generation from renewable sources such as wind and solar [1]. The primary challenge to fully transition to renewables is their inherent intermittency in production. To bridge the gap between energy demand and supply, scalable energy storage systems and flexible power generation systems such as gas turbines are needed [5]. Highly efficient gas turbines can ramp up and down with relative ease and can be utilized to match the fluctuations in peak power demand when renewables fall short in their supply [6]. Gas turbines will continue to be an integral component of future energy systems either as standalone systems, as flexible power sources, or for co-generation applications.

The fuel used in the combustion chambers of gas turbines, such as natural gas, leads to CO_2 emissions (contributed to 22% of fuel combustion emissions in 2021 [2]). Hydrogen's zero carbon emissions make it a promising combustion fuel, and industries worldwide are exploring design modifications to achieve efficient and reliable fuel-flexible combustors with an increasing proportion of hydrogen. However, hydrogen combustion poses significant challenges of flashback and higher NOx emissions [7]. In order to reduce NOx emissions, industrial combustion chambers are operated under lean premixed conditions. Hydrogen flames have a higher risk of flashback when operated at such conditions due to their high laminar flame speeds (nearly five times higher than natural gas at atmospheric conditions [8]). Also, the low Lewis number of hydrogen (indicative of its high diffusivity) at lean conditions and increased temperatures can lead to local enrichment, thereby increasing the combustion rate of hydrogen [9]. Local high concentrations of hydrogen can also lead to an increased propensity for flashback, especially close to the walls and stagnation point of the swirling flow in swirl-stabilized combustors [10, 11]. Hence, a detailed understanding of these combustors' underlying flow field physics is crucial to balance the competing requirements for hydrogen-air mixing.

The use of CFD has become an integral component in these complex combustors' design and optimization process. The commonly used approaches are URANS and Scale-Resolving Simulations (SRS) such as LES and hybrid RANS/LES methods [12]. URANS models are widely used in industries due to their low computational costs [13–15]. This approach decomposes the flow variables into a mean and fluctuating component, resulting in unknown quantities that need modelling. Closure models used for determining these unknowns provide information only on the statistical mean quantities, which is insufficient to describe the unsteady dynamics of turbulent combustion [16]. In order to accurately model the temporal evolution of the flow field, SRS methods are employed in analyzing combustors [17–22]. In LES, the flow variables are separated into large- and small-scale turbulent structures using filtering operation [23]. The large-scale turbulent eddies are resolved while the filtering operation introduces unknowns in the governing equations for which subgrid-scale (SGS) models are used [16]. However, LES explicitly resolves a larger portion of the energy spectrum than URANS, reducing the dependency on closure models. In industrial wall-bounded turbulent flows, the length scale of eddies in the near wall region is orders of magnitude lower than the bulk. High spatial and temporal resolution is needed in such regions, leading to increased computational costs, making classical LES prohibitive for such flows [24]. Alternatively, hybrid models such as the algebraic WMLES reduce the Reynolds number dependency on mesh resolution close to the walls, leading to lower computational times than classical LES [25]. In this approach, RANS formulation is used in the inner part of the logarithmic layer close to the walls, while a modified LES formulation is used in the outer part of the boundary layer [26].

Irrespective of the modelling approach used, combustion occurs by molecular mixing of fuel and oxidizer at the unresolved dissipative length scales. Consequently, the closure methods used for turbulent combustion modelling are similar for both URANS and SRS methods despite their differences in scale resolution, and most URANS combustion closure methods can be adapted for SRS [16]. Therefore, accurate predictions of unsteady turbulent flow statistics (velocity, pressure, and scalar concentration) are crucial for ensuring the validity and reliability of combustion predictions and associated emissions through the closure methods. In the SRS approach, the large-scale eddies which significantly impact the scalar mixing (thereby affecting the global flame properties and associated instabilities) are explicitly resolved instead of being averaged and hence provide more accurate predictions of turbulent mixing than URANS methods [27–29]. In addition, URANS predictions for shear-driven fuel-air mixing layers (as encountered in non-premixed/partially premixed combustors) are not accurate [30]. These inaccuracies arise due to the underlying assumption of universal applicability of closure coefficients in URANS equations primarily calibrated for highly idealized flow configurations [31]. These coefficients assume homogeneous and isotropic turbulence, which does not exist in the development regions of non-ideal jet flow configurations [32]. Also, thermal and density gradients (such as hydrogen-air systems) lead to additional modelling challenges in URANS methods [33–35]. Consequently, closure methods for turbulent chemical reaction rates produce non-physical combustion predictions due to inaccurate scalar mixing predictions. Hence, the use of SRS approach is preferred to predict unsteady mixing and resulting combustion accurately [16].

The computational time for the SRS approach is orders of magnitude higher than URANS due to higher grid/time-step resolution and long integration time scales to obtain ensemble-averaged solutions [15, 17]. Until such high computational power (massively parallel CPUs and GPUs) becomes widely accessible, industries will continue to rely on URANS prediction despite their lower accuracy. In this study, CFD simulations of shear-driven hydrogen-air mixing in the radial swirl stabilized DLE combustor of the OP16 gas turbine [36] are performed using URANS and WMLES approaches without including reaction mechanisms.

The main focus is to compare hydrogen/air mixing at different locations of the combustor using URANS and WMLES prediction methods.

2. OP16 DLE COMBUSTOR

The OP16 gas turbine (Figure 1) rated at 1.9MW is of an all-radial design [37]. The all-radial turbine is, by its nature, robust, making it suitable for burning challenging fuels. The lack of intricate cooling geometries in the hot flow path makes the OP16 suitable for alternative fuels. The combustion system consists of four tubular combustors mounted in a reverse flow direction. The engine is fitted with a specific type of combustor depending on the application [38].

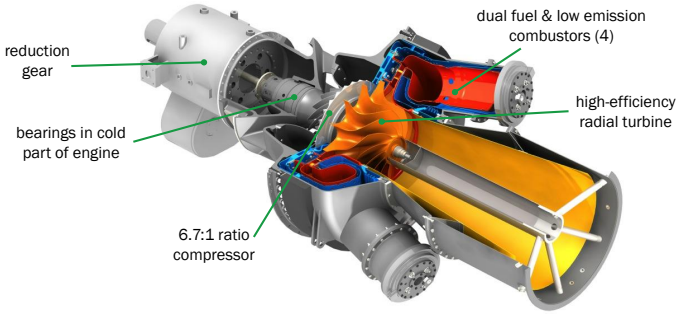

FIGURE 1: The OP16 gas turbine (courtesy of Destinus Energy).

In the present study, the radial swirl stabilized DLE combustor is chosen for the analysis (isometric CAD view in Figure 2 and schematic of the flow-field in cross-sectional view in Figure 3). It is operated in (partially) premixed mode to reduce emissions. The compressor discharge air heats up while cooling the combustion liner, favourably increasing the air supply temperature to the mixing zone. The fuel is injected via the main fuel inlet upstream of the swirler blades (Pilot fuel is not considered in the present study). The radial swirler blades induce a recirculation zone, stabilizing the combustion flame. Air addition through the dilution holes ensures an even temperature distribution level of combustion products before entering the turbine.

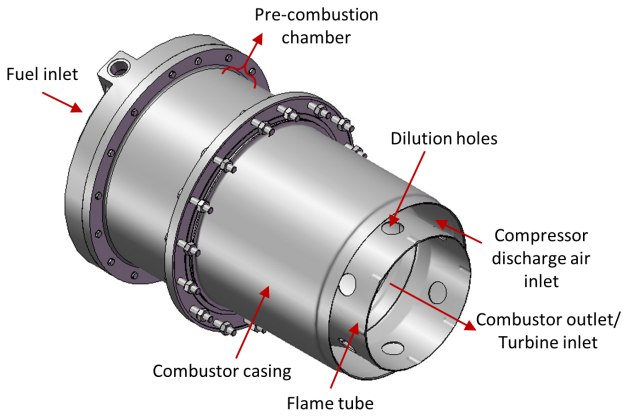

FIGURE 2: Isometric CAD view of the OP16 DLE combustor (courtesy of Destinus Energy).

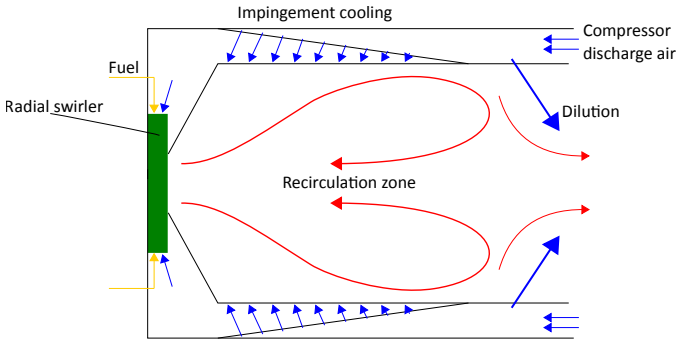

FIGURE 3: Cross-sectional representation of the flow-field in the OP16 DLE combustor: Schematic visualization (courtesy of Destinus Energy).

3. NUMERICAL MODELLING

Taking advantage of the rotational symmetry of the DLE combustor, CFD simulations are performed on one-eighth of the geometry. This simplification introduces two additional periodic boundary faces in the domain. Critical regions for mixing, such as the fuel inlet, swirler blades' suction side, and its leading/trailing edges, are positioned away from the periodic face to ensure negligible influence of the periodicity assumption on mixing. The current study does not consider the cooling liner, and the air inlet's inflow conditions are adjusted accordingly. Polyhedral meshes are generated using the Fluent Watertight Meshing Workflow of Ansys 2021R2. Figure 4 shows a coarse mesh for visualization purposes.

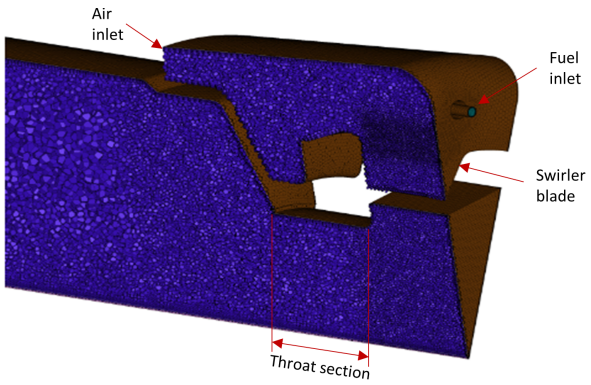

FIGURE 4: Visual representation of the simplified OP16 DLE combustor mesh consisting of 4.7 million polyhedral cells (URANS and WMLES simulations are performed on mesh densities of 6.2 and 21.6 million polyhedral cells, respectively).

The flow governing equations are the Navier-Stokes equation coupled with transport equations for total enthalpy H and species mass fraction Y (without chemical reaction term). They can be expressed as [16]:

$$\frac{\partial \rho}{\partial t} + \frac{\partial \rho u_j}{\partial x_j} = 0 \tag{1}$$

$$\frac{\partial \rho u_i}{\partial t} + \frac{\partial \rho u_j u_i}{\partial x_j} = -\frac{\partial p}{\partial x_i} + \frac{\partial \tau_{ij}}{\partial x_j} + F_i \tag{2}$$

$$\frac{\partial \rho H}{\partial t} + \frac{\partial \rho u_j H}{\partial x_j} = \frac{\partial p}{\partial t} + \frac{\partial}{\partial x_j}\left(\mathcal{J}_j^h + u_i \tau_{ij}\right) + u_j F_j \quad (3)$$

$$\frac{\partial \rho Y_k}{\partial t} + \frac{\partial \rho u_j Y_k}{\partial x_j} = -\frac{\partial \mathcal{J}_j^k}{\partial x_j} \quad (4)$$

Here, τ_{ij} represents the viscous force tensor, F_i is body force, $\mathcal{J}_j^k$ is the molecular diffusive flux of the species k and H denotes the total enthalpy. Since significant density gradients exist in the flow, the governing equations are Favre (mass-weighted) averaged and filtered in the URANS and the SRS approaches [16], respectively.

The Favre averaging procedure in URANS leads to unknowns such as the Reynolds stresses, species/temperature turbulent fluxes, and laminar diffusive fluxes [16]. The Reynolds stress term is modelled using the Shear Stress Transport (SST) based $k-\omega$ eddy-viscosity model with curvature correction due to its better flow predictions of swirling flows over the standard $k-\epsilon$ model (based on the studies by [39–42]). Detailed mathematical treatment of this model along with modelling coefficients can be found in [43, 44]. The gradient transport hypothesis is used for turbulent fluxes, which depends on turbulent viscosity (obtained from the turbulence model) and the turbulent Schmidt number.

Similarly, Favre filtering of the governing equations in LES results in unknown quantities such as the unresolved Reynolds stresses, unresolved species fluxes, and filtered laminar diffusion fluxes [16]. The Smagorinsky SGS modelling [45] is used for determining unresolved stresses. In order to avoid resolving the small scales of eddies in the near wall region, the zonal two-layer model - Wall Modelled LES (WMLES) approach is employed. The sub-grid scale viscosity is calculated with RANS formulation in the near-wall region and Smagorinsky SGS model away from it. This can be expressed as [26]:

$$\mu_t = \min\left\{(\kappa y)^2, (C_s \Delta)^2\right\} f_d |S| \quad (5)$$

Where κ is the von Karman constant (0.41), y is the wall distance, C_s is the Smagorinsky constant (0.1 in the present study based on the work of [46]), Δ is the sub-grid length scale, f_d is the wall-dampening function [47] and $|S|$ is the strain rate tensor. The minimum function leads to the Prandtl-van Driest mixing length model in the near-wall region and the Smagorinsky SGS model away from it.

The thermophysical properties of air and hydrogen are given as temperature-dependent polynomial functions in the operating temperature range [48]. The mixture properties are calculated using the volume-weighted mixing law. In both the modelling approaches, the SIMPLE algorithm is used for pressure-velocity coupling and second-order upwind schemes are used for energy, species, and turbulent quantities with the bounded second-order implicit transient formulation. For momentum discretization, a second-order upwind scheme is used by URANS, while WMLES employs a bounded second-order implicit scheme. The computations are performed on ANSYS Fluent 2021R2 version.

The mesh used for URANS and WMLES simulations consist of approximately 6.2 and 21.6 million polyhedral cells, respectively (Table 1). The mesh independence study for URANS and the turbulent kinetic energy (TKE) resolved in WMLES approach are discussed in the subsequent section. In WMLES simulations, a constant time step of 2×10^{-7}s is used such that the CFL number is 4.1 in the region within three nozzle diameter lengths from the fuel inlet (accounts for 0.4% by volume of the fuel-air mixing region) and the CFL $\leq$ 0.4 in the rest of the domain. The time-step size in URANS is chosen to be an order of magnitude higher than WMLES, i.e. 2×10^{-6}s (based on [27, 49]), leading to CFL $\leq$ 1.6 (CFL number within three nozzle diameters is 6.8). The number of parallel CPU cores (Xeon E5-2680 v4) used for computations and their associated computational expense is detailed in Table 1.

TABLE 1: Computational mesh size, time-step size and CPU hours for URANS and WMLES simulations (maximum CFL refers to CFL number in the region not enclosed within three nozzle diameters lengths from the fuel inlet)

	URANS	WMLES
Mesh size (cells)	6,210,492	21,601,663
Time step (s)	2×10^{-6}	2×10^{-7}
max. CFL	1.6	0.4
CPU hours	13,165	94,408

4. RESULTS

The mixing predictions of URANS and WMLES simulations are compared at four regions of interest as indicated in Table 2 along with the definitions of non-dimensional coordinates at each location. These planes are schematically shown in Figure 5 where d_f is the fuel inlet diameter, y^* and z^* represent the wall-normal height and length at the *Swirler plane* (highlighted in orange in Figure 5) non-dimensionalized using the swirler blade chord length C and R is the combustor radius.

TABLE 2: Plane locations and non-dimensional coordinates

Plane	Location	Non -dimensional Coordinates
X1, X2	Fuel-air mixing region	y/d_f, z/d_f
Swirler plane	Pressure side of Swirler blade	$y^* = y/C$, $z^* = z/C$
Z1	Trailing edge of swirler blade	x/C
X3, X4, X5	Throat section	z/R

The concentration of H_2 is represented by its equivalence ratio ϕ. Turbulent kinetic energy (TKE) k and axial velocity u along x are non-dimensionalized using the TKE and velocity of incoming air respectively ($k^* = \rho\widetilde{u_i'' u_i''}/\rho U_{air}^2$, u/U_{air}). The Unmixedness level (ψ) of hydrogen and air at a given location is the ratio of the standard deviation of equivalence ratio (σ_ϕ) and the mean equivalence ratio at that location (ϕ_{mean}). This can be expressed as:

$$\psi = \frac{\sigma_\phi}{\phi_{\text{mean}}} \quad (6)$$

Where, $0 \leq \psi \leq 1$, with $\psi = 0$ representing homogeneously mixed hydrogen-air ($\sigma_\phi = 0$), while $\psi = 1$ represents the pure air

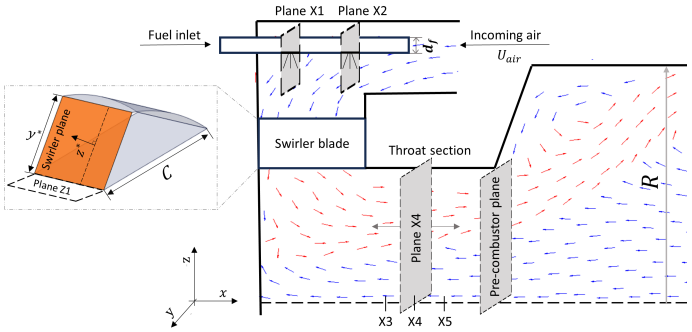

FIGURE 5: Schematic location of the planes and swirler blade's non-dimensional coordinates. d_f is the fuel inlet diameter, C refers to the swirler blade chord length, and R is the combustor radius. Vectors represent the tangential projection of the swirling flow onto the zx plane along the positive (red) and negative (blue) axial (x) directions.

stream (no hydrogen; $\phi_{\text{mean}} = 0$).

The mesh-independence study for the URANS approach was performed on five different mesh densities ranging from 3.1 million to 21.6 million cells with a constant time step size of 2×10^{-6}s. These meshes were evaluated based on the radial profiles of time-averaged fuel-equivalence ratio (ϕ) and axial velocity (u/U_{air}) predictions at *Plane X4* (Figure 6). The maximum deviation in the equivalence ratio and axial velocity predictions between 6.2 million and 21.6 million meshes is 2.8% and 3.6%, respectively. Considering an increase in computational expense of nearly three times for 21.6 million cells (37,010 CPU hours) compared to 6.2 million cells (13,165 CPU hours), a mesh size of 6.2 million cells is used for the URANS approach.

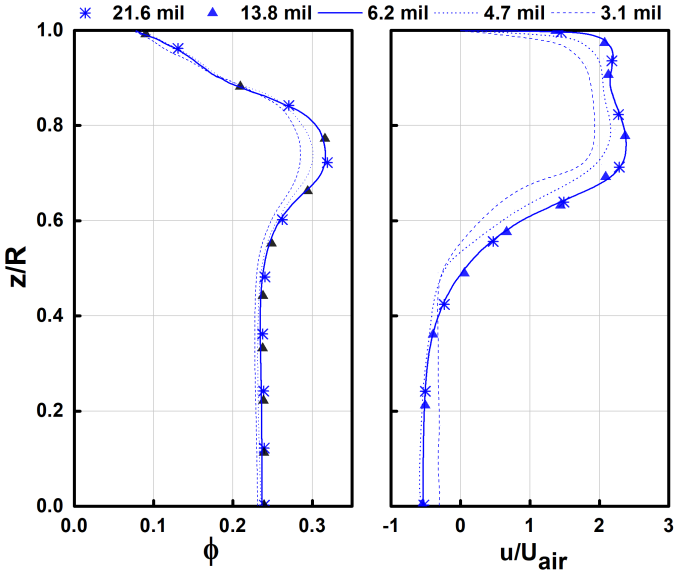

FIGURE 6: Radial profiles of time-averaged URANS prediction of equivalence ratio (ϕ) and axial velocity (u/U_{air}) along the radial direction (z/R) at *Plane X4* on different mesh densities.

In order to assess the mesh for WMLES simulations, the minimum ratio of resolved TKE (k_{res}) to total TKE ($k_{\text{total}} = k_{\text{res}} + k_{\text{sgs}}$, where k_{sgs} refers to modelled sub-grid scale TKE) is evaluated in the region of interest including the fuel-air mixing region, swirler blade region and the throat section for three different mesh densities as indicated in Table 3. The time-step size is chosen such that the maximum CFL number is 0.4 in the domain (this analysis does not include the region enclosed within three nozzle diameter lengths from the fuel inlet). The 21.6 million cells mesh is used for the WMLES simulations since it explicitly resolves higher fraction of TKE ($k_{\text{res}}/k_{\text{total}} \geq 0.7$) and satisfies the wall-normal resolution requirement of $\Delta y^+ \sim 1$ [50] at the swirler blade and the throat sections (at the fuel inlet $\Delta y^+ \sim 1.8$).

TABLE 3: Computational time and minimum resolved TKE in WMLES simulations on different mesh densities at maximum CFL of 0.4 (region enclosed within three nozzle diameters lengths from the fuel inlet not analyzed)

	6.2 mil	13.8 mil	21.6 mil
Mesh size (cells)	6,210,492	13,838,212	21,601,663
Time step (s) (max. CFL: 0.4)	6.7×10^{-7}	4.8×10^{-7}	2×10^{-7}
CPU hours	40,805	61,115	94,408
min. $k_{\text{res}}/k_{\text{total}}$	0.48	0.57	0.71

At *Planes X1* and *X2*, mixing occurs as the incoming air encounters the hydrogen jet exiting from the fuel inlet. These interacting fluid streams have high gradients of flow variables (velocity, pressure, temperature, and density). The mixing is due to shear layer entrainment at the interface of the fluid streams and the highly diffusive nature of hydrogen. The time-averaged $\phi = 1$ iso-line predictions by both modelling approaches at these planes are shown in Figure 7.

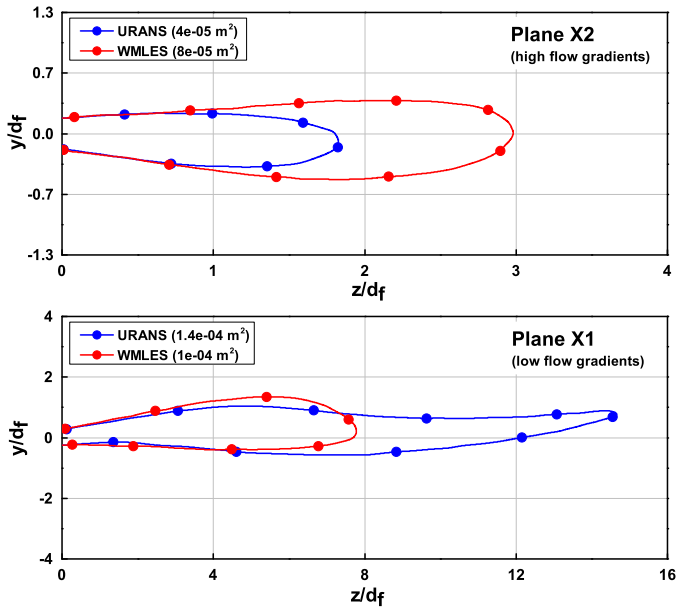

FIGURE 7: URANS and WMLES predictions of time-averaged $\phi = 1$ iso-lines at *Planes X1* and *X2*. Surface area enclosed within each iso-line is represented in brackets.

The area within the iso-lines has a higher concentration of hydrogen (i.e. $\phi > 1$). The higher the surface area enclosed within the $\phi = 1$ iso-line, the lower the mixing rate with the surrounding air stream. The gradients of flow variables between hydrogen and air streams are the highest at *Plane X2*, where fresh fuel and air interact in a "cross-flow" configuration (air stream is directed along the negative x direction while the hydrogen exiting the fuel inlet is normal to it). As the fuel and air mix, the gradients decrease along the negative x direction. Consequently, the surface area enclosed within the $\phi = 1$ iso-line will be lower at *Plane X2* (high mixing) compared to further downstream of the fuel inlet at *Plane X1* (lower mixing). This is evident from the area enclosed within $\phi = 1$ iso-line at these two planes in Figure 7. At *Plane X2*, URANS over-predicts mixing compared to WMLES, while a reverse trend is observed at *Plane X1*, where the penetration depth of $\phi = 1$ iso-line is significantly higher in URANS than in WMLES. A similar analysis was performed for multiple planes along the fuel inlet, and at every location, mixing predictions in WMLES are higher than URANS, with the highest differences observed at *Plane X1*.

The fuel-air shear layers interact along the swirler blade, leading to a spatial variation of ϕ in this region. Zones of high equivalence ratio in the near-wall region (low velocities) of swirler blades could be prone to BLF, evaluated along the *Swirler plane*. Figure 8 shows the plot of wall-normal distance (y^*) at which $\phi = 0.3$ (critical equivalence ratio of hydrogen for BLF based on [10]) along the length of the swirler blade (z^*). Based on the WMLES results, the trailing edge of the swirler blade ($z^* = 0.5$) could be prone to BLF, while URANS predicts a lower equivalence ratio and, consequently, a lower risk of BLF at this location.

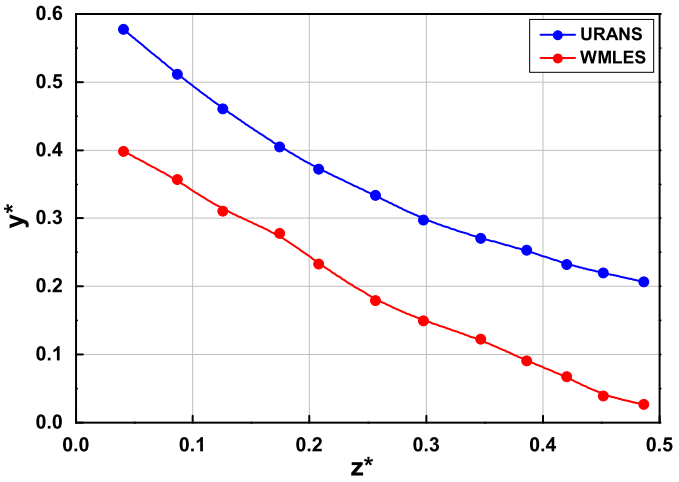

FIGURE 8: URANS and WMLES predictions of time-averaged ϕ = 0.3 iso-line near the *Swirler plane*. y^* and z^* represent the non-dimensionalized wall normal height and swirler blade length.

The degree to which the interaction of shear layers achieves uniformity in mixing is analyzed in terms of the unmixedness (ψ) at the trailing edge of the swirler blade at *Plane Z1*. The time-averaged equivalence ratio ϕ is plotted along the non-dimensional width (x/C) of the swirler blade as shown in Figure 9 (ϕ at a given x is averaged along y). Mixing is underestimated in URANS ($\psi = 0.3$) by 50% compared to WMLES ($\psi = 0.15$) with significant differences at *Plane X1* (similar observation in Figure 7). The non-dimensional TKE (k^*) is plotted at the same location as shown in Figure 10. At *Plane X1*, k^* is under-predicted in URANS compared to WMLES, and the scalar mixing predictions also follow the same trend.

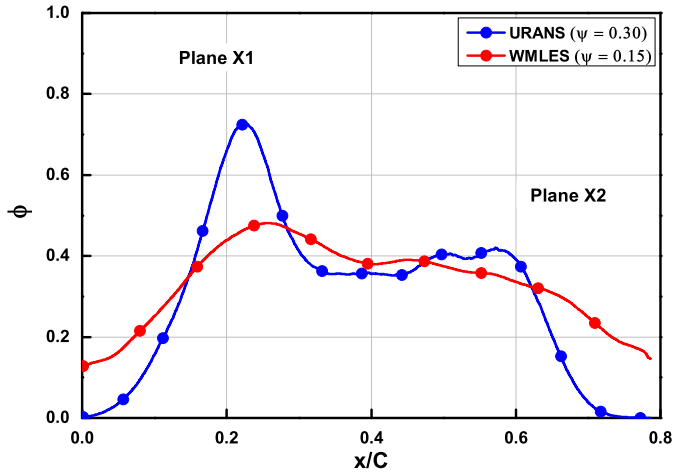

FIGURE 9: URANS and WMLES predictions of time-averaged equivalence ratio (ϕ) and Unmixedness (ψ) along the swirler blade width (x/C) at *Plane Z1*.

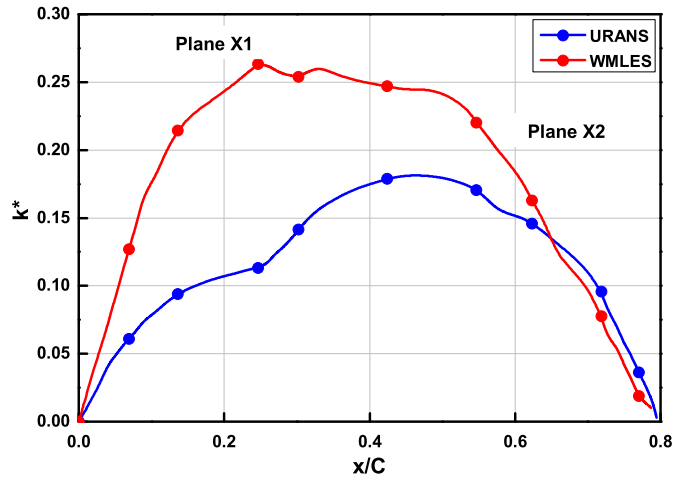

FIGURE 10: URANS and WMLES predictions of time-averaged non-dimensional TKE (k^*) along the swirler blade width (x/C) at *Plane Z1*.

In URANS approach, the Favre averaging of molecular diffusive flux $\mathcal{J}_j^k$ in Equation 4 yields unknown laminar ($\overline{\mathcal{J}_j^k}$) and turbulent ($\bar{\rho}\widetilde{u_j'' Y_k''}$) diffusive fluxes where the former is negligible compared to the latter. The turbulent diffusive flux is expressed using a gradient transport hypothesis with a linear dependence on turbulent viscosity (μ_t) as [16]:

$$\bar{\rho}\widetilde{u_j'' Y_k''} = -\frac{\mu_t}{Sc_t}\frac{\partial \tilde{Y}_k}{\partial x_j} \tag{7}$$

Where Sc_t represent turbulent Schmidt number, which has a constant value of 0.7 (based on [51]) in the present study. In the SST-based $k-\omega$ model, k and μ_t are linked through the transport equation for TKE (k) [43]. Hence, predictions of TKE directly influence the species turbulent diffusivity and the overall mixing patterns in the system.

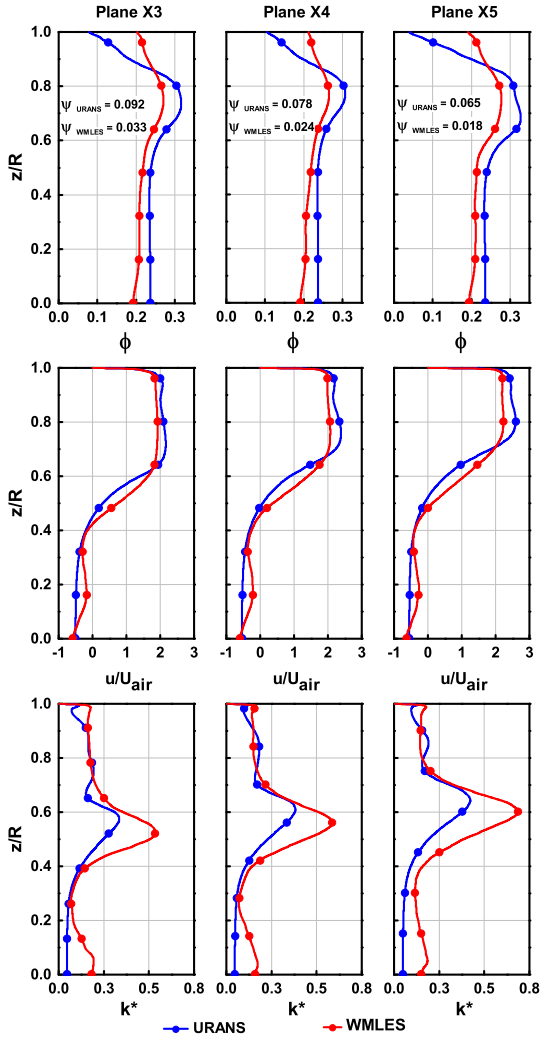

FIGURE 11: Radial profiles of time-averaged URANS and WMLES predictions of equivalence ratio (ϕ), axial velocity (u/U_{air}) and TKE (k^*) along the radial direction (z/R) at *Planes X3 - X5*.

Hydrogen-air mixtures from each of the swirler blades impinge on each other, generating a swirling flow enhancing fuel-air mixing along the throat section with a central recirculation zone. The radial profiles of time-averaged fuel-equivalence ratio (ϕ), axial velocity (u/U_{air}) and TKE (k^*) are plotted at Planes 3 - 5 in the throat section as shown in Figure 11. Although the velocity profile shape predictions are similar in both the modelling approaches, URANS over-predicts the recirculation region diameter (z value at $u/U_{air} = 0$) by nearly 22% across the throat section compared to WMLES (similar observation in the works of [49, 52]). Both u/U_{air} and k^* are under-predicted close to the shearing region of the fuel-air mixture (positive values of u/U_{air} between zero and linear velocity profile), leading to a lower level of mixing in URANS compared to WMLES as evident from the unmixedness (ψ) values at each of these planes.

The instantaneous fuel equivalence ratio contour is plotted in Figure 12 where the time-averaged mixing level is under-predicted by 74% in URANS (ψ = 0.054) compared to WMLES (ψ = 0.014). NOx emission predictions and the propensity for BLF in this region will be significantly higher in the URANS approach due to higher unmixedness and equivalence ratio near the combustor walls (Figure 12) compared to WMLES. Similar under predictions of TKE and passive scalar mixing predictions in swirling flows were made in the works of [53, 54]. However, in the present study, the differences are larger in magnitude, possibly due to the additional effects caused by the high-density gradient between hydrogen and air. The highly diffusive nature of hydrogen and high-density gradients in the system could lead to additional underlying physics, which are not accounted for by URANS-based methods, introducing uncertainty and limitations in the accuracy of predictions.

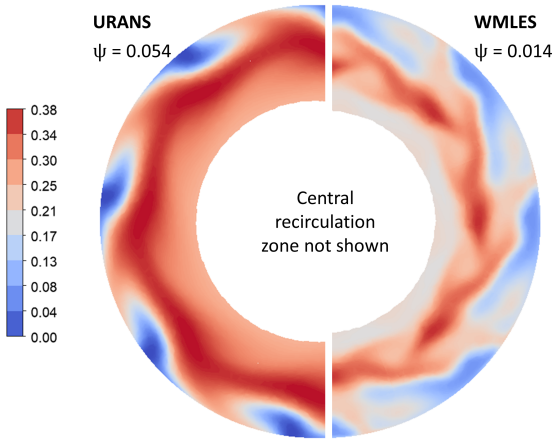

FIGURE 12: URANS (left) and WMLES (right) predictions of instantaneous equivalence ratio (ϕ) contour at the pre-combustor plane. Central recirculation zone is not shown.

5. CONCLUSION AND FUTURE WORK

In this study, shear-driven turbulent mixing of hydrogen and air in the OP16 DLE combustor has been investigated using the SST-based $k-\omega$ (URANS) and WMLES methods. The TKE predictions are lower in URANS than WMLES, leading to significant differences in the hydrogen-air mixing level (unmixedness) in both approaches. This can be attributed to modelling the growth and interactions of the shear layers using coefficients developed for homogeneous isotropic turbulence in URANS methods. Such assumptions do not hold for non-ideal jet flow configurations encountered in swirl-stabilized combustors. Also, literature studies [54–56] have shown the deficiencies of a constant turbulent Schmidt number assumption across the flow field and that its variation alone would not yield accurate results. Therefore, URANS models suffer from assumptions in both eddy-viscosity and mixing models.

The major limitation of the present study is the lack of experimental data to compare and validate the CFD predictions. In addition to this, other limitations are (i) the impact of high CFL

number close to the fuel inlet (three nozzle diameter lengths) on the potential core length of the hydrogen jet and its impact on mixing in the downstream region is unknown, (ii) URANS simulations have been performed with a time-step size corresponding to a maximum CFL of 1.6. However, the implicit time stepping scheme used in URANS is known to be numerically stable at higher time steps and is not restricted by CFL < 1 criteria [57, 58]. The use of higher time steps would lead to a reduction in computational expense for URANS, and (iii) the periodicity assumption may not accurately represent the turbulent flow structures close to the boundary, leading to inaccuracies in the energy spectrum and possible suppression of turbulence close to the boundary face. However, as WMLES resolves the large-scale structures, it provides more information on the unsteady turbulent flow than URANS. The differences in predictions of the two approaches highlight the importance of explicitly resolving turbulent scales in such complex systems.

More comprehensive studies on shear-driven turbulent mixing of hydrogen-air systems are needed, both experimentally and numerically. Simulations at different combustor load conditions and Reynolds number of the fuel inlet must be performed to assess their influence on the scalar mixing predictions. Additionally, the role of higher molecular diffusivity of hydrogen in such turbulent flow conditions should be further analyzed and compared with different fuels. The local flow properties must be accounted for in URANS models to improve their predictions rather than assuming the closure coefficients to be universally valid, irrespective of the flow type. Such additional terms/corrections will significantly benefit industries in performing efficient and reliable URANS simulations to address modelling challenges associated with hydrogen combustion systems.

6. ACKNOWLEDGEMENT

The project has received financial support from TKI Energie under grant number: TKI-2021-H2-23.

REFERENCES

[1] Ritchie, Hannah, Roser, Max and Rosado, Pablo. "Energy." Our World in Data (2023). URL https://ourworldindata.org/energy.

[2] "Greenhouse Gas Emissions from Energy Data Explorer." IEA (2023). URL https://www.iea.org/data-and-statistics/data-tools/greenhouse-gas-emissions-from-energy-data-explorer.

[3] "Climate strategies and targets-2050 long-term strategy." EU Commission and others (2018). URL https://climate.ec.europa.eu/eu-action/climate-strategies-targets_en.

[4] "Global Energy Review: CO2 Emissions in 2021." IEA (2022). URL https://www.iea.org/reports/global-energy-review-co2-emissions-in-2021-2.

[5] Gils, Hans Christian, Scholz, Yvonne, Pregger, Thomas, de Tena, Diego Luca and Heide, Dominik. "Integrated modelling of variable renewable energy-based power supply in Europe." *Energy* Vol. 123 (2017): pp. 173–188. URL https://doi.org/10.1016/j.energy.2017.01.115.

[6] Gonzalez-Salazar, Miguel Angel, Kirsten, Trevor and Prchlik, Lubos. "Review of the operational flexibility and emissions of gas-and coal-fired power plants in a future with growing renewables." *Renewable and Sustainable Energy Reviews* Vol. 82 (2018): pp. 1497–1513. URL http://dx.doi.org/10.1016/j.rser.2017.05.278.

[7] Gupta, Krishna Kumar, Rehman, Ameenur and Sarviya, RM. "Bio-fuels for the gas turbine: A review." *Renewable and Sustainable Energy Reviews* Vol. 14 (2010): pp. 2946–2955. URL https://doi.org/10.1016/j.rser.2010.07.025.

[8] Ravi, Sankaranarayanan and Petersen, Eric L. "Laminar flame speed correlations for pure-hydrogen and high-hydrogen content syngas blends with various diluents." *International journal of hydrogen energy* Vol. 37 No. 24 (2012): pp. 19177–19189. URL https://doi.org/10.1016/j.ijhydene.2012.09.086.

[9] Vance, Faizan Habib, Shoshin, Yuriy, de Goey, Philip and van Oijen, Jeroen. "Flame stabilization and blow-off of ultra-lean H2-air premixed flames." *Energies* Vol. 14 No. 7 (2021): p. 1977. URL https://doi.org/10.3390/en14071977.

[10] Klein, Sarakatsanis C., S. "Validation of Hydrogen Boundary Layer Flashback Model on Gas Turbine Geometries and Conditions." *Proceedings of ASME Turbo Expo 2022 Turbomachinery Technical Conference and Exposition*. GT2022- 79816: p. 4916. Rotterdam, Netherlands, July 13–17, 2022. URL https://doi.org/10.1115/GT2022-79816.

[11] Björnsson, Klein S. A., Ó. H. and Tober, J. "Boundary Layer Flashback Model for Hydrogen Flames in Confined Geometries Including the Effect of Adverse Pressure Gradient." *ASME. J. Eng. Gas Turbines Power* Vol. 143 No. 6 (2021): p. 061003. URL https://doi.org/10.1115/1.4048566.

[12] Vilag, Valeriu, Vilag, Jeni, Carlanescu, Razvan, Mangra, Andreea and Florean, Florin. *CFD application for gas turbine combustion simulations*. IntechOpen, London, UK (2019).

[13] Kiesewetter, Konle M., F. and Sattelmayer, T. "Analysis of Combustion Induced Vortex Breakdown Driven Flame Flashback in a Premix Burner With Cylindrical Mixing Zone." *ASME. J. Eng. Gas Turbines Power* Vol. 129 (2007): pp. 929–936. URL https://doi.org/10.1115/1.2747259.

[14] Joung, D. and Huh, K. Y. "3D RANS Simulation of Turbulent Flow and Combustion in a 5 MW Reverse-Flow Type Gas Turbine Combustor." *ASME. J. Eng. Gas Turbines Power* Vol. 132 (2010): p. 111504. URL https://doi.org/10.1115/1.2747259.

[15] Ebrahimi, Houshang B. "Overview of Gas Turbine Augmentor Design, Operation, and Combustion Oscillation." *42nd AIAA/ASME/SAE/ASEE Joint Propulsion Conference Exhibit*. AIAA 2006-4916: p. 4916. Sacramento, California, July 9–12, 2006. DOI 10.2514/6.2006-4916. URL https://arc.aiaa.org/doi/pdf/10.2514/6.2006-4916.

[16] Veynante, Denis and Vervisch, Luc. "Turbulent combustion modeling." *Progress in energy and combustion science* Vol. 28 No. 3 (2002): pp. 193–266. URL https://doi.org/10.1016/S0360-1285(01)00017-X.

[17] Gicquel, Laurent YM, Staffelbach, Gabriel and Poinsot, Thierry. "Large eddy simulations of gaseous flames in gas turbine combustion chambers." *Progress in energy and*

combustion science Vol. 38 No. 6 (2012): pp. 782–817. URL https://doi.org/10.1016/j.pecs.2012.04.004.

[18] Fureby, Christer. "LES of a multi-burner annular gas turbine combustor." *Flow, turbulence and combustion* Vol. 84 (2010): pp. 543–564. DOI 10.1007/s10494-009-9236-9.

[19] Kim, Won-Wook, Menon, Suresh and Mongia, Hukam C. "Large-eddy simulation of a gas turbine combustor flow." *Combustion Science and technology* Vol. 143 No. 1-6 (1999): pp. 25–62. URL https://doi.org/10.1080/00102209908924192.

[20] Selle, Laurent, Lartigue, Ghislain, Poinsot, Thierry, Koch, R, Schildmacher, K-U, Krebs, W, Prade, B, Kaufmann, P and Veynante, Denis. "Compressible large eddy simulation of turbulent combustion in complex geometry on unstructured meshes." *Combustion and Flame* Vol. 137 No. 4 (2004): pp. 489–505. URL https://doi.org/10.1016/j.combustflame.2004.03.008.

[21] Lv, Guangpu, Liu, Xiao, Zhang, Zhihao, Li, Shengnan, Liu, Enhui and Zheng, Hongtao. "Large eddy simulations of pilot-stage equivalence ratio effects on combustion instabilities in a coaxial staged model combustor." *Physics of Fluids* Vol. 35 No. 9 (2023): p. 095134. URL https://doi.org/10.1063/5.0169437.

[22] Patil, S. and Tafti, D. "Large-Eddy Simulation of Flow and Convective Heat Transfer in a Gas Turbine Can Combustor With Synthetic Inlet Turbulence." *ASME. J. Eng. Gas Turbines Power* Vol. 134 No. 7 (2012): p. 071503. URL https://doi.org/10.1115/1.4006081.

[23] Ghosal, Sandip and Moin, Parviz. "The basic equations for the large eddy simulation of turbulent flows in complex geometry." *Journal of Computational Physics* Vol. 118 No. 1 (1995): pp. 24–37. URL https://doi.org/10.1006/jcph.1995.1077.

[24] Pope, Stephen B. "Ten questions concerning the large-eddy simulation of turbulent flows." *New journal of Physics* Vol. 6 No. 1 (2004): p. 35. DOI 10.1088/1367-2630/6/1/035.

[25] Sagaut, Pierre, Terracol, Marc and Deck, Sebastien. *Multiscale and multiresolution approaches in turbulence-LES, DES and Hybrid RANS/LES Methods: Applications and Guidelines*. World Scientific, Singapore (2013).

[26] Nikitin, NV, Nicoud, Franck, Wasistho, B, Squires, KD and Spalart, Philippe R. "An approach to wall modeling in large-eddy simulations." *Physics of fluids* Vol. 12 No. 7 (2000): pp. 1629–1632. URL https://doi.org/10.1063/1.870414.

[27] Sadiki, Amsini, Maltsev, A, Wegner, B, Flemming, F, Kempf, A and Janicka, J. "Unsteady methods (URANS and LES) for simulation of combustion systems." Vol. 45 No. 8 (2006): pp. 760–773. URL https://doi.org/10.1016/j.ijthermalsci.2005.11.001.

[28] Benim, Iqbal S Nahavandi A Meier W Wiedermann A Joos F., AC. "Analysis of Turbulent Swirling Flow in an Isothermal Gas Turbine Combustor Model." *Proceedings of the ASME Turbo Expo 2014: Turbine Technical Conference and Exposition. Volume 4A: Combustion, Fuels and Emissions*. GT2014-25008. Düsseldorf, Germany, June 16–20, 2014. URL https://doi.org/10.1115/GT2014-25008.

[29] Tangermann, Eike and Pfitzner, Michael. "Evaluation of combustion models for combustion-induced vortex breakdown." *Journal of Turbulence* Vol. 10 No. 7 (2009): pp. 1–21. URL https://doi.org/10.1080/14685240802592423.

[30] Yoder, Dennis A, DeBonis, James R and Georgiadis, Nicholas J. "Modeling of turbulent free shear flows." *Computers & fluids* Vol. 117 (2015): pp. 212–232. URL https://doi.org/10.1016/j.compfluid.2015.05.009.

[31] Bradshaw, P. "Turbulence modeling with application to turbomachinery." *Progress in Aerospace Sciences* Vol. 32 No. 6 (1996): pp. 575–624. URL https://doi.org/10.1016/S0376-0421(96)00003-6.

[32] Wilcox, David C. *Turbulence modeling for CFD*. DCW industries, Canada (1998).

[33] Georgiadis, Nicholas J and DeBonis, James R. "Navier–Stokes analysis methods for turbulent jet flows with application to aircraft exhaust nozzles." *Progress in Aerospace Sciences* Vol. 42 No. 5-6 (2006): pp. 377–418. URL https://doi.org/10.1016/j.paerosci.2006.12.001.

[34] Bush, Robert H, Chyczewski, Thomas S, Duraisamy, Karthikeyan, Eisfeld, Bernhard, Rumsey, Christopher L and Smith, Brian R. "Recommendations for future efforts in RANS modeling and simulation." *AIAA Scitech 2019 Forum*. AIAA 2006-4916: p. 0317. San Diego, California, January 7–11, 2019. DOI 10.2514/6.2019-0317.

[35] Morgan, Brandon E. "Scalar mixing in a Kelvin-Helmholtz shear layer and implications for Reynolds-averaged Navier-Stokes modeling of mixing layers." *Physical Review E* Vol. 103 No. 5 (2021): p. 053108. URL https://doi.org/10.1103/PhysRevE.103.053108.

[36] Ramaekers, Wilhelmus JS, Tap, Ferry A, Bouten, Thijs WFM and Axelsson, Lars-Uno. "Comparison of Different CFD Models for Predicting Emissions in an OPRA DLE Combustor." *Proceedings of the ASME Turbo Expo 2019: Turbomachinery Technical Conference and Exposition. Volume 4B: Combustion, Fuels, and Emissions*. GT2019-91317, V04BT04A019. Phoenix, Arizona, USA, June 17-21, 2019. URL https://doi.org/10.1115/GT2019-91317.

[37] Axelsson, Lars-Uno, van Groenewoud, Ruud and Stulp, Mark. "Operational experience of the OP16 gas turbine in small scale CHP installations in Europe." URL https://www.destinus.energy/download_resources/#row-number-5.

[38] Bouten, Thijs, Withag, Jan and Axelsson, Lars-Uno. "Hydrogen–A key enabler for the energy transition." *White Paper*. URL https://www.destinus.energy/download_resources/#row-number-5.

[39] Meziane, Sidahmed and Bentebbiche, Abdelhalim. "Numerical study of blended fuel natural gas-hydrogen combustion in rich/quench/lean combustor of a micro gas turbine." *International Journal of Hydrogen Energy* Vol. 44 No. 29 (2019): pp. 15610–15621. URL https://doi.org/10.1016/j.ijhydene.2019.04.128.

[40] Kashir, Babak, Tabejamaat, Sadegh and Jalalatian, Nafiseh. "A numerical study on combustion characteristics of blended methane-hydrogen bluff-body stabilized swirl dif-

fusion flames." *International Journal of Hydrogen Energy* Vol. 40 No. 18 (2015): pp. 6243–6258. URL https://doi.org/10.1016/j.ijhydene.2015.03.023.

[41] Vigueras-Zuniga, Marco-Osvaldo, Tejeda-del Cueto, Maria-Elena, Vasquez-Santacruz, José-Alejandro, Herrera-May, Agustín-Leobardo and Valera-Medina, Agustin. "Numerical predictions of a swirl combustor using complex chemistry fueled with ammonia/hydrogen blends." *Energies* Vol. 13 No. 2 (2020): p. 288. URL https://doi.org/10.3390/en13020288.

[42] AbdelGayed, HM, Abdelghaffar, WA and El Shorbagy, K. "Flame vortex interactions in a lean premixed swirl stabilized gas turbine combustor–Numerical computations." *American Journal of Scientific and Industrial Research* Vol. 4 No. 5 (2013): pp. 449–467. DOI 10.5251/ajsir.2013.4.5.449.467.

[43] Menter, F. R. "Two-equation eddy-viscosity turbulence models for engineering applications." *AIAA Journal* Vol. 32 No. 8 (1994): pp. 1598–1605. DOI 10.2514/3.12149.

[44] Esch, T. "Heat transfer predictions based on two-equation turbulence models with advanced wall treatment." *Turbulence Heat Mass Transf* Vol. 4 (2003): pp. 633–640.

[45] Smagorinsky, Joseph. "General circulation experiments with the primitive equations: I. The basic experiment." *Monthly weather review* Vol. 91 No. 3 (1963): pp. 99–164. URL https://doi.org/10.1175/1520-0493(1963)091%3C0099:GCEWTP%3E2.3.CO;2.

[46] Branley, N and Jones, WP. "Large eddy simulation of a turbulent non-premixed flame." *Combustion and Flame* Vol. 127 No. 1-2 (2001): pp. 1914–1934. URL https://doi.org/10.1016/S0010-2180(01)00298-X.

[47] Piomelli, Ugo, Moin, Parviz and Ferziger, Joel H. "Model consistency in large eddy simulation of turbulent channel flows." *The Physics of fluids* Vol. 31 No. 7 (1988): pp. 1887–1891. URL https://doi.org/10.1063/1.866635.

[48] Lemmon, Eric, Huber, Marcia and McLinden, Mark. "NIST Standard Reference Database 23: Reference Fluid Thermodynamic and Transport Properties-REFPROP." Version 8.0. Natl Std. Ref. Data Series (NIST NSRDS) (2007). Accessed February 4, 2007, URL https://www.nist.gov.

[49] Dunham, Spencer-A-McGuirk JJ Dianat M., D. "Comparison of URANS and LES CFD Methodologies for Air Swirl Fuel Injectors." *Proceedings of the ASME Turbo Expo 2008: Power for Land, Sea, and Air.* GT2008-50278: pp. 187–196. Berlin, Germany, June 9–13, 2008. URL https://doi.org/10.1115/GT2008-50278.

[50] Menter, Florian, Schutze, J, Kurbatskii, K, Lechner, R, Gritskevich, Mikhail and Garbaruk, Andrey. "Scale-Resolving simulation techniques in industrial CFD." *6th AIAA Theoretical Fluid Mechanics Conference*. AIAA 2011-3474: p. 3474. Honolulu, Hawaii, June 27–30, 2011. URL https://doi.org/10.2514/6.2011-3474.

[51] Hernandez, Wang-Q-McDonell V Mansour A Steinthorsson E Hollon B., SR. "Micro Mixing Fuel Injectors for Low Emissions Hydrogen Combustion." *Proceedings of the ASME Turbo Expo 2002: Power for Land, Sea, and Air*. GT2008-50854: pp. 675–685. Berlin, Germany, June 9–13, 2008. URL https://doi.org/10.1115/GT2008-50854.

[52] Wankhede, Tap-FA-Schapotschnikow P Ramaekers WJS., MJ. "Numerical Study of Unsteady Flow-Field and Flame Dynamics in a Gas Turbine Model Combustor." *Proceedings of the ASME Turbo Expo 2014: Turbine Technical Conference and Exposition.* GT2014-25784: pp. 675–685. Düsseldorf, Germany, June 16–20, 2014. URL https://doi.org/10.1115/GT2014-25784.

[53] Galeazzo, Donnert G. Habisreuther P. Zarzalis N. Valdes R. J., F. C. C. and Krebs, W. "Measurement and Simulation of Turbulent Mixing in a Jet in Crossflow." *ASME. J. Eng. Gas Turbines Powe.* Vol. 133 No. 6 (2011): p. 061504. URL https://doi.org/10.1115/1.4002319.

[54] Ivanova, Elizaveta, Noll, Berthold and Aigner, Manfred. "RANS and LES of turbulent mixing in confined swirling and non-swirling jets." *6th AIAA Theoretical Fluid Mechanics Conference*. AIAA 2011-3934: p. 3934. Honolulu, Hawaii, June 27–30, 2011. URL https://doi.org/10.2514/6.2011-3934.

[55] Jiang, Lei-Yong and Campbell, Ian. "Prandtl/Schmidt number effect on temperature distribution in a generic combustor." *International Journal of Thermal Science* Vol. 48 No. 2 (2009): pp. 322–330. URL https://doi.org/10.1016/j.ijthermalsci.2008.03.014.

[56] Andreini, Antonio, Facchini, Bruno, Innocenti, Alessandro and Cerutti, Matteo. "Numerical analysis of a low NOx partially premixed burner for industrial gas turbine applications." *Energy Procedia* Vol. 45 (2014): pp. 1382–1391. URL https://doi.org/10.1016/j.egypro.2014.01.145.

[57] Matsson, John E. *An Introduction to Ansys Fluent 2023*. SDC Publications, USA (2023).

[58] Dunham, David. "Unsteady fluid mechanics of annular swirling shear layers." Ph.D. Thesis, Loughborough University, Loughborough, United Kingdom. 2011. URL https://hdl.handle.net/2134/8483.

[59] You, Yonghua, Seibold, Florian, Wang, Sheng, Weigand, Bernhard and Gross, Ulrich. "URANS of turbulent flow and heat transfer in divergent swirl tubes using the k-ω SST turbulence model with curvature correction." *International Journal of Heat and Mass Transfer* Vol. 159 (2020): p. 120088. DOI 10.1016/j.ijheatmasstransfer.2020.120088.

[60] Schneider, E, Maltsev, A, Sadiki, A and Janicka, J. "Study on the potential of BML-approach and G-equation concept-based models for predicting swirling partially premixed combustion systems: URANS computations." *Combustion and Flame* Vol. 152 No. 4 (2008): pp. 548–572. DOI https://doi.org/10.1016/j.combustflame.2007.10.013.

[61] Poinsot, Thierry and Veynante, Denis. *Theoretical and numerical combustion*. RT Edwards, Inc., Australia (2005).

[62] Fric, Thomas F. "Effects of fuel-air unmixedness on NO(x) emissions." *Journal of Propulsion and Power* Vol. 9 No. 5 (1993): pp. 708–713. URL https://doi.org/10.2514/3.23679.